RSC Advances

PAPER

View Article Online
View Journal | View Issue

Cite this: *RSC Adv.*, 2017, **7**, 34857

Preparation of hollow Nd/TiO_2 sub-microspheres with enhanced visible-light photocatalytic activity

Jinlong Li,* Shuaiqiang Jia, Guozhe Sui, Lijuan Du and Boxin Li

Hollow Nd-doped TiO_2 sub-microspheres are synthesised *via* a controlled hydrolysis reaction, where carbon spheres are employed as the template. The building blocks of TiO_2 doped with Nd are deposited on the surface of carbon spheres and subsequently, the carbon spheres are removed by calcination in air. The structure and morphology of the hollow Nd/TiO_2 sub-microsphere composites are characterised by X-ray diffraction (XRD), Fourier-transform infrared spectroscopy (FT-IR), scanning electron microscopy (SEM), transmission electron microscopy (TEM), low temperature N_2 adsorption (Brunauer–Emmett–Teller analysis), simultaneous thermal analysis (TG-DTA), diffuse reflectance UV-vis spectroscopy (DRS) and X-ray photoelectron spectroscopy (XPS). The SEM and TEM micrographs reveal that the as-prepared hollow Nd/TiO_2 sub-microsphere composite has an average diameter of 100 nm and a special uniform morphology, where the hollow sub-microspheres are constructed by TiO_2 nano-chains, which resemble cage-like structures. The Nd-doped Nd/TiO_2 composites exhibit high visible light absorption capacity, high adsorption ability and high photocatalytic activity towards Rhodamine B (RhB). Further, the effect of neodymium content on the physical structure and photocatalytic properties of hollow Nd/TiO_2 sub-microspheres is investigated. Finally, it is concluded that the higher photocatalytic performance of as-prepared hollow Nd/TiO_2 sub-microspheres stems from their hollow structure comprised of Nd/TiO_2 nanostructures and a high light-harvesting efficiency.

Received 9th May 2017
Accepted 6th July 2017

DOI: 10.1039/c7ra05228f

rsc.li/rsc-advances

1. Introduction

Environmental pollution is one of the most serious problems facing humanity today. The potential of air pollution to cause illness and even death has led to increased public concern. Recently, semiconducting photocatalytic materials such as ZnO, SnO_2, ZrO_2 and TiO_2 have been applied widely for the degradation of toxic organic and inorganic pollutants in wastewater.[1–10] Among these semiconductor photocatalysts, TiO_2 has been proven as the most suitable material, with potential for wide-spread application in tackling environmental challenges. As a promising semiconductor photocatalyst, TiO_2 has attracted worldwide interest owing to its long-term biological and chemical stabilities, compatibility with other materials, strong oxidising power and environmentally friendly nature.[11–13]

Despite these positive characteristics, however, several problems associated with TiO_2 limit the practicality of its application, namely a large band gap (3.2 eV), limited adsorption of solar light and low photocatalytic activity arising from the fast recombination of charge carriers.[14] In general, less than 5% of solar irradiation can be captured by the Earth's surface, which imposes a limit on the optical absorption in the UV region of the solar spectrum.[15] Furthermore, the fast recombination rate of the generated charge carriers, in combination with the slow transfer rate of electrons to oxygen, limit the efficiency of TiO_2 as a photocatalyst.[16] It is well established that photocatalytic activity can be enhanced by adjusting the band structure of the corresponding material to improve its visible-light response and charge separation. For this reason, the design and development of a photocatalyst that could be activated under irradiation with visible light is essential.

In order to achieve improved photocatalytic performance, various TiO_2 photocatalysts with different structures and morphologies, including nanowires,[17,18] nanorods,[19] nanotubes,[20,21] microspheres,[22] porous structures,[23] and hollow microspheres,[24–27] have been synthesised to date. Among these, hollow TiO_2 microspheres have attracted more notable attention than other nanoparticles owing to their higher specific surface area, higher photocatalytic activity, higher light collection efficiency and special structure. Therefore, the development of materials and technologies for the fabrication of hollow TiO_2 microspheres, which is aimed at enhancing absorption in the visible spectral range,[28,29] has become one of the new important challenges in the field of photocatalysis. Similarly, doping of titania with rare earth metal or lanthanide metal ions[30–32] has also attracted considerable attention. In particular, doping with lanthanide ions with 4f electron configurations has the potential to significantly enhance the photocatalytic activity of TiO_2. Margan *et al.* have shown[33] that Cd-doped anatase TiO_2

College of Chemistry and Chemical Engineering, Qiqihar University, Qiqihar 161006, China. E-mail: jinlong141@163.com; Fax: +86-452-2738205; Tel: +86-452-2738205

with a higher photocatalytic activity than that of P25 TiO_2 can be prepared *via* sol–gel method. Zhang *et al.* reported[34] that earth metal ions (Zr/Co) modified significantly the band structure of TiO_2, thus resulting in improved photocatalytic behaviour. This method not only extended the photo-response to the visible region, it also improved the separation efficiency of photo-induced electron–hole pairs of TiO_2.[35] In particular, doping with Nd ions has proven to be an efficient method for enhancing the photoactivity of TiO_2 towards selected reactions.

In this paper, hollow Nd/TiO_2 sub-microspheres with a high photocatalytic activity are prepared using a very simple and straightforward synthetic method. In this method, carbon spheres were prepared as a template and subsequently, hollow Nd/TiO_2 sub-microspheres were fabricated by controlled hydrolysis and calcination. The photocatalytic activity of the as-prepared photocatalyst towards the degradation of Rhodamine B (RhB) in aqueous solution was comprehensively studied.

2. Experimental

2.1 Materials and chemicals

Glucose ($C_6H_{12}O_6$) was used to synthesise carbon spheres. Titanium trichloride ($TiCl_3$) was used as the titanium precursor in the synthesis of nanocrystalline TiO_2. Neodymium nitrate ($Nd(NO_3)_3 \cdot 6H_2O$) was used as the metal precursor for doping TiO_2. These chemicals, together with hydrogen chloride solution (HCl, 36.5 wt%), ethanol (CH_3CH_2OH), sodium bicarbonate ($NaHCO_3$), *tert*-butyl alcohol ($C_4H_{10}O$), methanol (CH_3OH), ρ-benzoquinone ($C_6H_4O_2$) and Rhodamine B (RhB, $C_{28}H_{31}N_2O_3Cl$) were analytical grade purchased from Sigma-Aldrich Co. Commercially available TiO_2 powder, Aeroxide® P25 TiO_2 (Evonik Degussa GmbH), which is well known to possess very high photocatalytic activity, was selected as the reference material for comparative studies. RhB was selected as the model dye for photocatalytic degradation experiments. All reagents were of analytical grade and were used as obtained without further purification. Distilled water was used in all experiments requiring water.

2.2 Synthesis of carbon sphere template

Glucose (60 mL, 0.5 mol L^{-1}) solution was sealed in a 100 mL stainless-steel autoclave and was maintained at 180 °C for 8 h. Subsequently, the solution was cooled to room temperature. The resulting black solid was collected and washed sequentially with deionised water, ethanol and acetone five times. Finally, the carbon spheres were obtained as a brown solid after drying at 80 °C for 8 h.

2.3 Synthesis of hollow Nd/TiO_2 sub-microspheres

A sample of as-prepared carbon spheres (0.2 g) was added to ethanol (120 mL) and the solution was ultrasonicated for 30 min, affording a mixture referred to as solution A. Meanwhile, a specified weight of $Nd(NO_3)_3 \cdot 6H_2O$ was dispersed in ethanol (10 mL), yielding solution labelled as B. Solution B was added drop-wise to solution A and the resulting mixture was stirred continuously for 30 min, followed by the addition of an aqueous solution of $TiCl_3$ (15 wt%, 2.0 mL) and HCl (6 mol L^{-1}, 2.0 mL). Subsequently, the mixed solution was heated to 98 °C and maintained at this temperature for 1 h. The Nd/TiO_2 sub-microsphere precursor was obtained after washing with distilled water and drying under vacuum at 105 °C for 10 h. Finally, hollow Nd/TiO_2 sub-microspheres were obtained after calcination in air at 550 °C for 2 h.

2.4 Characterisation

X-ray power diffraction (XRD) measurements were performed on a Bruker D8 instrument, allowing the determination of the phase composition and structure of samples with Cu Kα radiation under 40 kV and 30 mA operating conditions in the range $2\theta = 20$–$80°$, with a speed of 4.00° min^{-1}. The specific surface areas of the photocatalysts (at a relative pressure ranging from 0.05–0.35) were determined using the Brunauer–Emmett–Teller (BET) approach using N_2 adsorption–desorption apparatus Nova 2000e (Quantachrome GmbH & Co.). Fourier-transform infrared (FT-IR) spectra were measured with an FT-IR spectrophotometer Nexus 670 (Nicolet Co.). Scanning electron microscopy (SEM) images were acquired with a Hitachi S-3400, operated at 100 kV. Transmission electron microscopy (TEM) images were obtained with a Hitachi (Japan) working at 200 kV. Thermogravimetric differential scanning calorimetry (TG-DSC) analysis was performed using a TG instrument 6200 (PE Co.) at a heating rate of 10 °C min^{-1} (30–1000 °C) under air atmosphere. Diffuse reflectance UV-vis spectroscopy analysis of dry-pressed disk samples was performed using a UV-visible spectrophotometer Du800 (Beckman Co.). $BaSO_4$ was used as a reflectance standard in the UV-vis diffuse reflectance experiments. X-ray photoelectron spectroscopy (XPS) images were obtained on an Axis Ultra DLD (Kratos Co.). The take-off angle of the photoelectron was kept at 45°. The binding energy was referenced by setting the C 1s hydrocarbon peak to 285.0 eV.

2.5 Evaluation of photocatalytic activity

The photocatalytic activities of hollow Nd/TiO_2 sub-microspheres towards the degradation of RhB in aqueous solutions were evaluated under visible light irradiation. A 500 W xenon lamp was used as the light source and the visible wavelength was controlled through a 420 nm glass cut filter, which was hanged in a dark box and kept on the top of photoreactor. The experiments were carried out with 50 mg of hollow Nd/TiO_2 sub-microspheres and 50 mL solution of RhB (5 mg L^{-1}) in a tube reactor. In each case, the suspension was magnetically stirred in the dark for 30 min, which allowed it to reach adsorption equilibrium prior to illumination. Subsequently, visible lamp was directed towards the suspension. Samples were withdrawn from the reactor at regular time intervals and centrifuged using a high-speed centrifuge (RG-TGL-16C, Ruijiang Co.) to remove the photocatalyst. The absorbance of the obtained filtrate was measured using a UV-vis spectrophotometer SP 1900 (Shanghai Spectrum Instruments Co.), with the absorbance at 552.0 nm used as the representative peak for RhB concentration.

2.6 Recycling test

After each photocatalytic experiment, recycling experiments were carried out *via* centrifuging and washing the composite with ethanol for 1 h under magnetic stirring. The recycled composite was used as catalysts to degrade RhB (5 mg L^{-1}), respectively. Reusability of the hollow Nd/TiO_2 sub-microspheres composite was investigated by repeating the experiment five times.

3. Results and discussion

3.1 Characterisation of hollow Nd/TiO_2 sub-microspheres

Fig. 1 shows the anatase-to-rutile phase transition behaviour observed in the X-ray diffraction patterns of Nd/TiO_2 sub-microspheres as a function of calcination temperature. In all XRD patterns of hollow Nd/TiO_2 sub-microspheres, the anatase phase has been established using a reference pattern (JCPDS card no. 21-1272) with characteristic peaks at $2\theta = 25.5°$, 38.1°, 48.6°, 54.2° and 63.1°. However, the XRD patterns of hollow Nd/TiO_2 sub-microspheres prepared at a calcination temperature < 400 °C exhibited lower crystallinity. The rutile phase appeared in the spectra of hollow Nd/TiO_2 sub-microspheres calcined at 600 °C, with peaks characteristic peaks observed at $2\theta = 27.5°$, 36.1°, 41.3°, 54.4° and 56.6°. Furthermore, the content of the rutile phase increased with increasing calcination temperature. It is well known that the transition from anatase to rutile phase in TiO_2 occurs typically at a temperature of less than 600 °C. The hollow Nd/TiO_2 sub-microspheres calcined at 500 °C displayed relatively high crystallinity. Therefore, the optimum calcination temperature was determined to be 500 °C since no peaks associated with the rutile phase were found in the spectra of samples prepared at this temperature.[36]

The N_2 adsorption–desorption isotherms of hollow Nd/TiO_2 sub-microspheres and P25 TiO_2 samples are portrayed in Fig. 2. According to IUPAC, all prepared samples exhibited type IV isotherms with H2 hysteresis loops, which suggests the presence of mesopores that can provide higher photocatalytic activity towards RhB.[37] Experimentally, the BET surface area of hollow Nd/TiO_2 sub-microspheres was estimated to be 76.1 m^2 g^{-1}, and is thus larger than that of P25 TiO_2 (46.4 m^2 g^{-1}). A large specific surface area is known to be critical to enhancing the activity of photocatalysts. For this reason, the increase in the specific surface area of the prepared sub-microspheres confirmed the positive influence of doping titania and the hollow structures of the photocatalyst with Nd. Most likely, the presence of Nd atoms leads to improved control over nucleation and growth of crystallites, as well as the formation of well-ordered structures.[38]

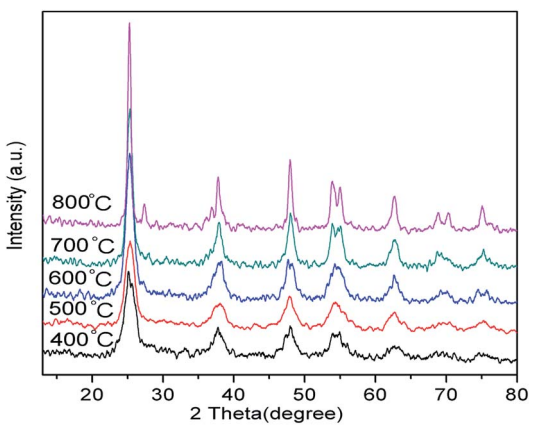

Fig. 1 XRD patterns of hollow Nd/TiO_2 sub-microspheres at different calcination temperatures.

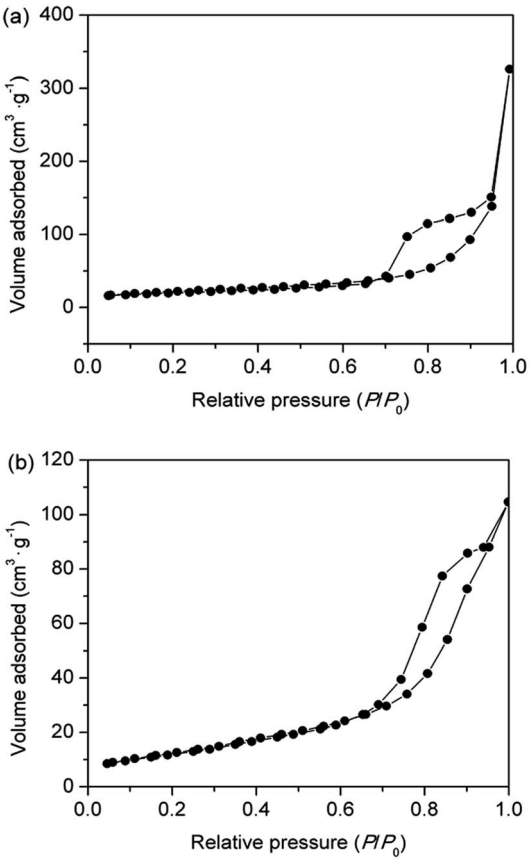

Fig. 2 N_2 adsorption–desorption isotherms of hollow Nd/TiO_2 sub-microspheres (a) and P25 TiO_2 (b).

The FT-IR analysis of hollow Nd/TiO_2 sub-microspheres was performed in the 400–4000 cm^{-1} range in order to ascertain the nature of the surface functional groups. The FT-IR spectra obtained for samples with and without the calcination step are shown in Fig. 3. The FT-IR spectra of all samples displayed a broad absorbance peak at around 3430 cm^{-1}, originating from the stretching vibrations of water or hydroxyl radicals. The spectrum of un-calcined hollow Nd/TiO_2 sub-microspheres (Fig. 3a) revealed the presence of two bands at 1691 cm^{-1} and 1592 cm^{-1}, which can be assigned to the stretching modes of C=C and C=O double bonds, respectively. The peak at 2927 cm^{-1} was assigned to the stretching vibrations associated with C–H bonds, and the peaks in the 1200–1300 cm^{-1} range were attributed to the C–OH stretching and O–H bending vibrations. The FT-IR spectra of hollow Nd/TiO_2 sub-microspheres after calcination are shown in Fig. 3b. The peak at 1630 cm^{-1} was assigned to the O–H stretching vibration of chemisorbed water.

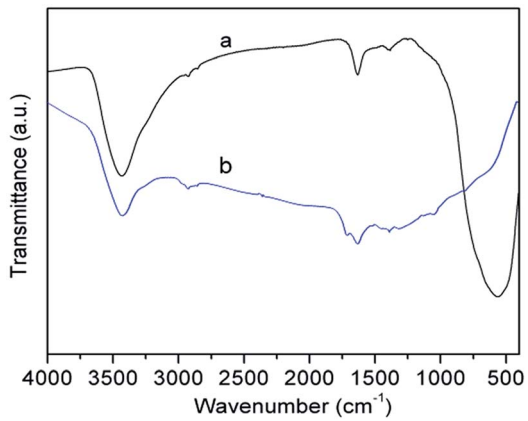

Fig. 3 FT-IR spectra of hollow Nd/TiO_2 sub-microspheres without calcinations (a) and with calcinations (b) at 500 °C.

The intensity of the absorption band in the region of 900–400 cm^{-1} could be assigned to the various stretching modes associated with metal oxides.[39] In this case, the band could be attributed to Ti–O and Nd–O bands in the Nd-doped TiO_2 samples. However, no peaks specific to Nd–O bands were evident, most likely as a result of the fact that the Nd content was below the limit of detection.

Fig. 4 shows the SEM and TEM images of carbon sphere templates and un-calcined Nd/TiO_2 sub-microsphere precursors. It is evident from the analysis of these images that the carbon templates were comprised of uniform sub-microspheres with approximately 200 nm in diameter (Fig. 4a and c). Fig. 4b and d show that all Nd/TiO_2 precursors synthesised through the hydrolysis process exhibited particles with very uniform morphology, with diameters ranging from 200 nm to 300 nm (referred to as sub-microspheres). Further, these figures show that the Nd/TiO_2 nanoparticles were dispersed uniformly on the surface of carbon sphere templates.

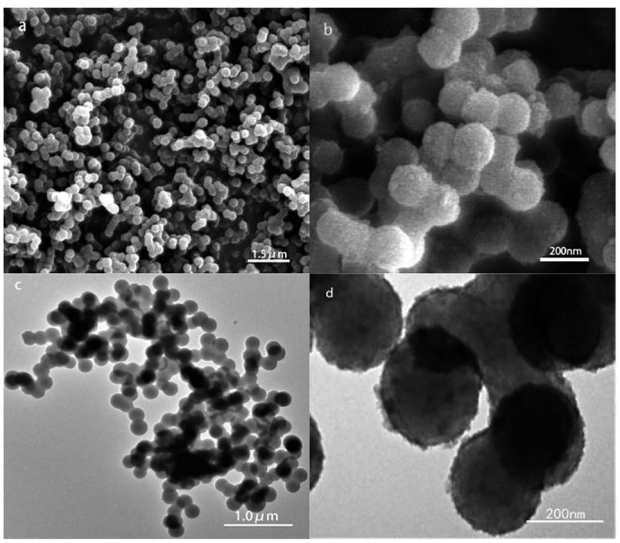

Fig. 4 SEM and TEM of carbon sphere templates (a, c) and Nd/TiO_2 submicrospheres without calcination (b, d).

The apparent adhesion between the precursors was attributed to the adsorption of amorphous TiO_2 generated by hydrolysis of Ti^{3+} on the surface of carbon spheres. The stable structures of the Nd/TiO_2 precursors facilitated in turn the formation of hollow sub-microspheres. Therefore, this analysis revealed that the utilisation of carbon microspheres as templates has allowed the formation of spherical shells with a relatively dense arrangement of thin Nd/TiO_2 nanolayers.

Fig. 5 shows the TEM images of hollow Nd/TiO_2 sub-microspheres obtained as a function of the concentration of the $TiCl_3$ solution employed in their synthesis. It can be seen that the concentration of $TiCl_3$ solution had a great impact on the morphology of Nd/TiO_2 composites. When the concentration of $TiCl_3$ solution was 0.015 M, the hollow spherical structures in the Nd/TiO_2 composites were not formed completely. As the concentration of the $TiCl_3$ solution increased to 0.021 M, a small amount of hollow microspheres was found to coexist with irregular structures. Formation of stable hollow spherical shell structures was observed in the material prepared using 0.042 M $TiCl_3$ solution. The diameters of these Nd/TiO_2 sub-microspheres after calcination were in the range of 100–120 nm, and were therefore smaller than those of the Nd/TiO_2 precursors coated on carbon microspheres. The decrease in particle size observed for the hollow structures was attributed to the removal of carbon microspheres as a result of calcination, and further increase in the density of loose TiO_2 precursor layers. The detailed images displayed in Fig. 5c clearly show that the surface of hollow Nd/TiO_2 sub-microspheres was very rough, with a large number of TiO_2 nanochains twisted together into a 3D assembly with a walnut-like structure. The successful formation of hollow Nd/TiO_2 sub-microspheres was determined by the presence of dark edges and bright centres in their TEM images. When the concentration of $TiCl_3$ solution was increased above 0.042 M, formation of a large quantity of Nd/TiO_2 nanoparticles, aggregated around carbon spheres, was observed instead.

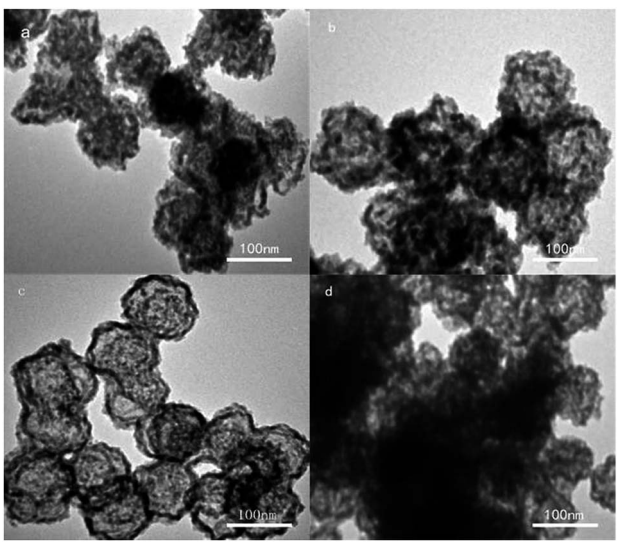

Fig. 5 TEM images of hollow Nd/TiO_2 sub-microspheres with different $TiCl_3$ concentration of 0.015 M (a), 0.021 M (b), 0.042 M (c), and 0.085 M (d).

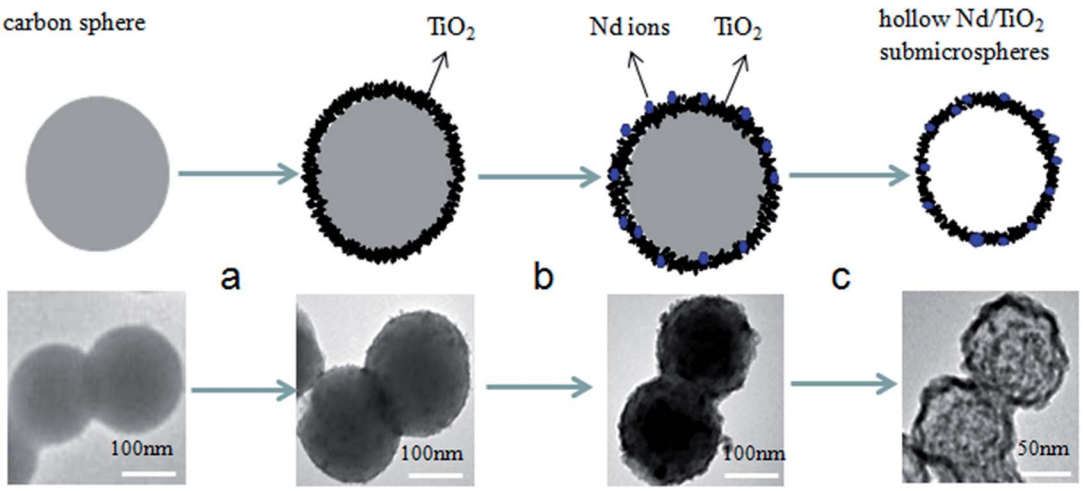

Fig. 6 Schematic illustration of the formation mechanism of hollow Nd/TiO_2 sub-microspheres.

Based on the above experimental results, a plausible mechanism for the formation of hollow Nd/TiO_2 sub-microspheres is proposed in Fig. 6. The carbon spheres are believed to have played a crucial role in controlling the morphology of the photocatalyst. TiO_2 nanoparticles were adsorbed on the surface of carbon spheres, partially aggregating with each. Simultaneously, a small amount of Nd ions was doped into the TiO_2 nanoparticles. Subsequently, the inner core of Nd/TiO_2 was removed by calcination, allowing hollow sub-microspheres to form gradually as the calcination progressed.

In order to find the most suitable calcination temperature for obtaining hollow Nd/TiO_2 sub-microspheres, TG-DSC analysis of the as-prepared Nd/TiO_2 precursors was conducted under nitrogen atmosphere. TG-DSC plots recorded under nitrogen at a heating rate of 2 °C min^{-1} are shown in Fig. 7. The TG curve revealed two main weight loss stages. The first weight loss of about 10% occurred between 50 °C and 250 °C, and was attributed to the evaporation of adsorbed water from the as-prepared Nd/TiO_2 precursors.[40] The second weight loss of about 50% occurred between 350 °C and 600 °C, and might be associated with the combustion of carbon spheres in air, resulting in the formation of hollow Nd/TiO_2 sub-microspheres. In addition, the appearance of two sharp exothermic peaks at about 107 °C and 520 °C in the DSC curve was in good agreement with the results of TGA analysis. These results showed that carbon spheres can be removed to a sufficient degree at a calcination temperature of 500 °C, allowing the formation of hollow structures.

Fig. 8 shows the UV-vis diffuse absorbance spectra of hollow Nd/TiO_2 sub-microspheres prepared with different contents of Nd. The results indicated that the introduction of Nd dopant gives rise to an obvious red shift in the absorption band edge associated with the hollow Nd/TiO_2 sub-microspheres. In addition, we observed that the red shift and visible absorbance of different samples changed as the content of Nd dopant increased. The noticeable red shift of the absorption edge to the visible light region could be ascribed to the following fact: the introduction of Nd atoms altered the energy levels of the TiO_2 band gap, and this new energy level induced the red-shift through a charge transfer mechanism between the impurity

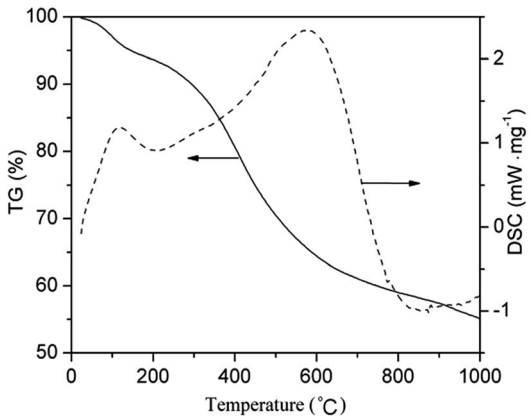

Fig. 7 TG-DSC curves of the hollow Nd/TiO_2 sub-microspheres.

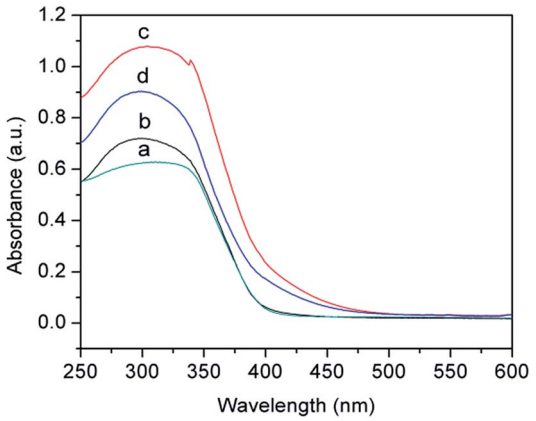

Fig. 8 DRS spectra of hollow sub-microspheres for TiO_2 (a), Nd/TiO_2 with 0.1 wt% Nd (b), Nd/TiO_2 with 0.2 wt% Nd (c), and Nd/TiO_2 with 0.3 wt% Nd (d).

and conduction bands of TiO_2.[41,42] This result can be also confirmed by the XPS spectra of hollow Nd/TiO_2 sub-microspheres. The peak positions of Ti $2p_{3/2}$ and Ti $2p_{1/2}$ shifted from 458.9 eV and 464.7 eV to 459.8 eV and 465.4 eV, respectively, as shown in Fig. 9b. Consequently, the outer electron cloud of Ti ions decreased due to the strong electron attraction of Nd atoms, and the energy gap was narrowed. When the content of Nd in the form of $Nd(NO_3)_3 \cdot 6H_2O$ was set at 0.2 wt%, the hollow Nd/TiO_2 sub-microspheres exhibited the strongest ultraviolet absorption ability, with a band gap of 3.02 eV. The formation of such a narrow energy gap was attributed to the movement of the top valence band position determined by the Nd 3d electron state to a shorter wavelength, and the movement of the bottom conduction band position determined by the Ti 2p state to a longer wavelength.[43] Therefore, this analysis showed that the addition of Nd may enhance the visible light photocatalytic performance of hollow Nd/TiO_2 sub-microspheres.

In the next step, the hollow Nd/TiO_2 sub-microspheres were analysed by XPS to examine the chemical states of different atoms (Fig. 9). The peaks visible in Fig. 9a showed that hollow Nd/TiO_2 sub-microspheres contain Ti, O, C and Nd atoms. However, the peak at 996.1 eV, ascribed to Nd 3d, was found to be quite weak as a result of the low content of Nd.[44]

Two major emission peaks were observed in the XPS spectra of Ti 2p at binding energies of 459.8 and 465.4 eV for Ti $2p_{3/2}$ and Ti $2p_{1/2}$, respectively, as shown in Fig. 9b. Comparison with standard XPS spectra revealed that these peaks arise form Ti^{4+} in the tetragonal structure of anatase TiO_2. As a consequence, it is possible to conclude that titanium within the hollow Nd/TiO_2 sub-microspheres exists predominantly in the Ti^{4+} form. In Fig. 9c, the strongest peak appeared at 531.1 eV and was ascribed to the lattice oxygen in the O^{2-} state, while the broad peak at around 533 eV was most likely arising as a result of the presence of water and hydroxide absorbed on the surface of hollow Nd/TiO_2 sub-microspheres. Fig. 9d showed that the doped Nd existed as Nd^{3+} in the hollow Nd/TiO_2 sub-microspheres, acting as an electron trapping centre.[45] Furthermore, two major peaks centred at 974.8 eV and 995.7 eV were observed, which represent Nd $3d_{5/2}$ and Nd $3d_{3/2}$ orbitals, respectively. Consequently, the doped Nd atoms abstract strongly electrons from the neighbouring Ti^{4+} cations, and the migration of these electrons from Ti ions results in a decrease in the density of the outer electron cloud of Ti ions.[46] Overall, this migration of electrons leads to a corresponding increase in the generation of the Ti^{3+} state. The existence of the Ti^{3+} state in turn retards the recombination of h^+ and e^-, which has a positive effect on the photocatalytic activity of hollow Nd/TiO_2 sub-microspheres. It can be concluded, therefore, that the metallic state of Nd produced a greater enhancement in the photocatalytic activity of TiO_2 by creating a Schottky barrier at the metal–semiconductor junction.[47]

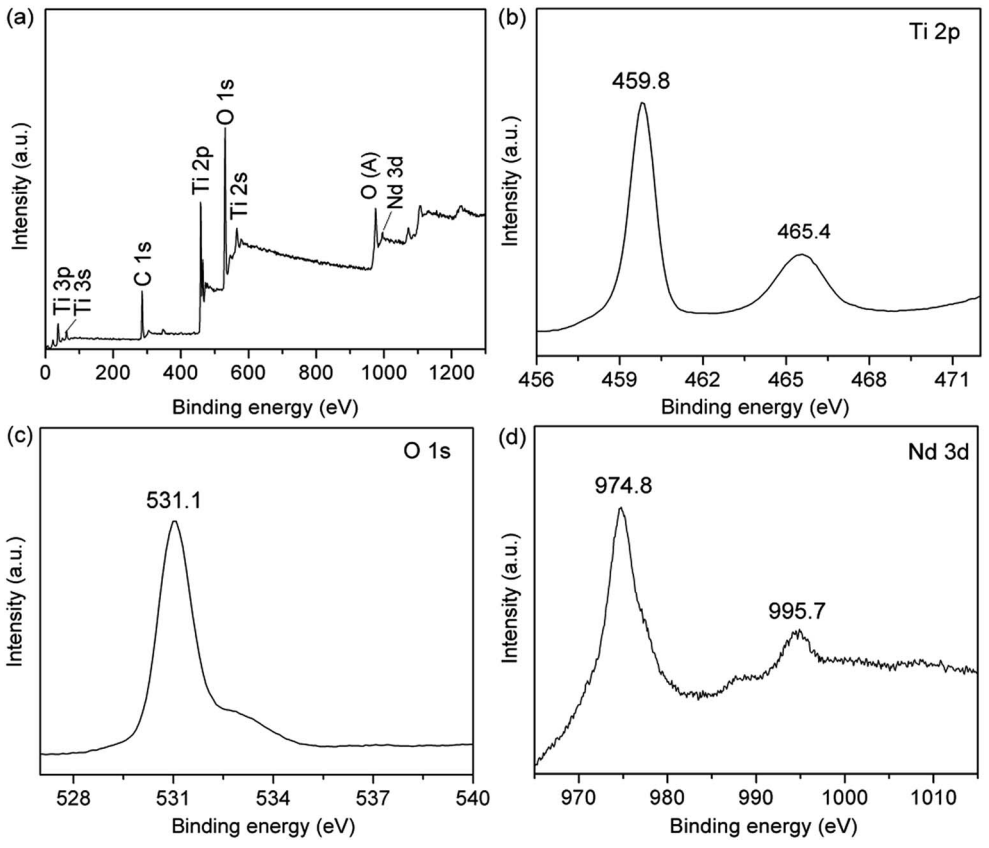

Fig. 9 XPS spectra of the hollow Nd/TiO_2 sub-microspheres: (a) survey spectrum, (b) Ti 2p spectrum, (c) O 1s spectrum, and (d) Nd 3d spectrum.

3.2 Photocatalytic activity

The photocatalytic activities of hollow TiO_2 sub-microspheres, hollow Nd/TiO_2 sub-microspheres with different Nd contents and P25 TiO_2 were evaluated by the degradation of an aqueous solution of RhB (50 mg L^{-1}) under illumination with visible light. As time progressed in these experiments, the RhB dye decomposed and the colour of the RhB solution became increasingly lighter. The photocatalytic degradation of RhB was calculated from the initial absorbance value of RhB in the solution (A_0) and the absorbance value of RhB at interval t (A_t) in terms of decolouration rate (η) of RhB as follow:

$$\eta = [(A_0 - A_t)/A_0] \times 100\%$$

Fig. 10 shows the photocatalytic activities of different samples determined under visible light illumination. The adsorption–desorption equilibria for all catalysts were achieved within 30 min of stirring in the absence of light. The adsorption percentages of RhB for the synthesised photocatalysts were around 5%, with the exception of 10% determined for P25 TiO_2. The hollow Nd/TiO_2 sub-microspheres with different Nd contents showed photocatalytic activities under visible light that were higher than those of P25 TiO_2 and hollow TiO_2 sub-microspheres, with the decolouration rates of samples with 0.1 wt%, 0.2 wt% and 0.3 wt% Nd contents determined as 92.4%, 93.5 and 91.1%, respectively, after visible light irradiation for 90 min. Therefore, this analysis revealed that the addition of Nd enhanced the visible light photocatalytic activity of the TiO_2 catalyst, which was consistent with the outcome of characterisation described above. In particular, the hollow Nd/TiO_2 sub-microspheres with 0.2 wt% of doped Nd exhibited the strongest photocatalytic activity. It is important to note that an appropriate content of Nd could result in increased presence of hydroxyls, which can in turn trap more photogenerated holes and improve the separation of electrons and holes. When the concentration of Nd^{3+} becomes too high, the space charge region becomes very narrow and Nd^{3+} may be served as a mediator of interfacial charge transfer or as a recombination

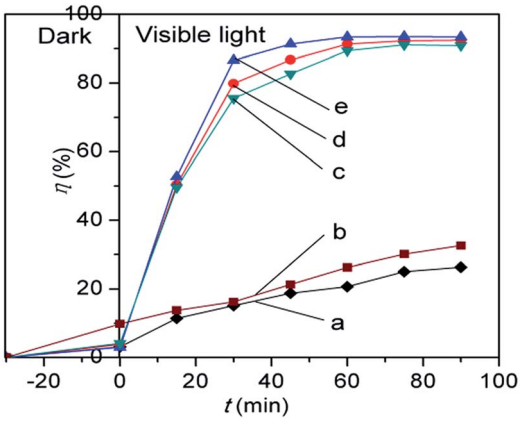

Fig. 10 Photocatalytic activities of hollow TiO_2 sub-microspheres (a), P25 TiO_2 (b), hollow Nd/TiO_2 sub-microspheres with 0.3 wt% Nd (c), 0.1 wt% Nd (d), and 0.2 wt% Nd (e).

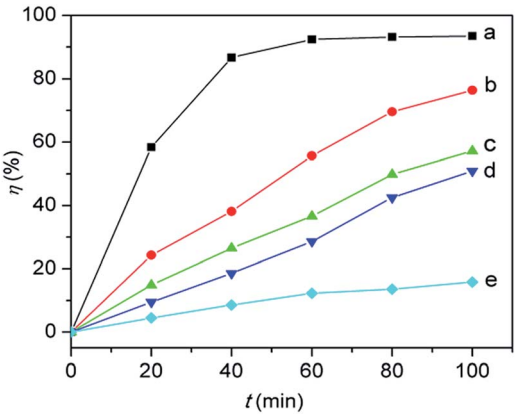

Fig. 11 Photocatalytic activities of RhB in 0.2 wt% Nd/TiO_2 hollow sub-microspheres suspension under visible irradiation with (a) no scavenger added, (b) 0.5 mM *p*-benzoquinone, (c) *tert*-butyl alcohol, (d) methanol, and (e) $NaHCO_3$. Scavenger concentration: 0.1 M.

center, so the recombination of the photogenerated electron–hole pairs in semiconductor becomes easier. And in our case the optimal content of Nd is 0.2 wt%, above which the photocatalytic activity decreases. Under visible light irradiation, a large number of photogenerated electrons in the valence band were transferred into the conduction band. At the same time, the TiO_2 molecules produced the same amount of photogenerated holes in the valence bands. And finally, all of these electrons and holes could migrate around the surface of the hollow Nd/TiO_2 sub-microspheres.

To confirm the reactive species during the photocatalytic reactions, sodium bicarbonate, *tert*-butyl alcohol, methanol, ρ-benzoquinone were added to the RhB solutions containing the hollow Nd/TiO_2 sub-microspheres composite, for the explanation of the role of the different species associated with degradation. As shown in Fig. 11, the degradation of RhB was obviously depressed by HCO_3^-, while it was slightly depressed by *tert*-butyl alcohol and methanol in the hollow Nd/TiO_2 sub-microspheres (0.2 wt% Nd) suspension. HCO_3^- can be adsorbed on the surface of catalyst and reacted with h^+ or $^{\bullet}OH$, leading to lower activity.[48] Because $^{\bullet}OH$ scavengers *tert*-butyl alcohol and methanol hardly adsorbed on the catalyst in aqueous systems, they mainly scavenged the free $^{\bullet}OH$ radical in RhB solution. Simultaneously, with the addition of $O_2^{\bullet-}$ scavenger *p*-benzoquinone, the degradation of RhB decreased to a certain degree, suggesting that $O_2^{\bullet-}$ was also the active species for RhB degradation in the present system. These results indicated that the surface adsorbed $^{\bullet}OH$ was the main reactive oxygen species in the photocatalytic reactions.

3.3 Reusability

To investigate the stability of the hollow Nd/TiO_2 sub-microspheres composite, cycling experiments were performed by washing the composite with ethanol for several times. The adsorption and photocatalytic performance of the hollow Nd/TiO_2 sub-microspheres composite for RhB (5 mg L^{-1}) solution by repeating the experiment five times, and the results are

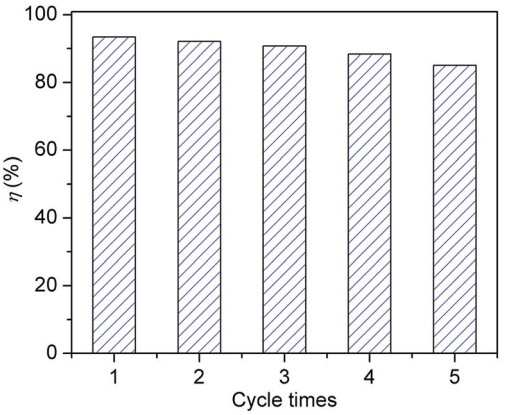

Fig. 12 Recycling of the hollow Nd/TiO_2 sub-microspheres photocatalyst in the removal of RhB dyes.

shown in Fig. 12. After five cycles, the removal efficiency decreases to 85.1% for RhB. This fact implies that the obtained hollow Nd/TiO_2 sub-microspheres composite have good stability and are less photo-corroded during the photocatalytic oxidation, which can be applied as a new options for dye wastewater treatment.

4. Conclusions

In summary, a hollow Nd/TiO_2 sub-microspheres photocatalyst was synthesised successfully using carbon spheres as templates through the hydrothermal method. The effects of several critical factors on the structure and photocatalytic properties of the prepared materials were evaluated. X-ray diffraction analysis showed that the hollow Nd/TiO_2 sub-microspheres produced at a calcination temperature of 500 °C consisted almost exclusively of the anatase phase. The hollow Nd/TiO_2 sub-microspheres exhibited higher efficiency and stability with respect to the decomposition of RhB than P25 TiO_2 under visible light irradiation. The interstitial Nd atoms within the TiO_2 lattice played an important role in generating intermediate energy levels and narrowing the band-gap, thereby enhancing the photocatalytic activity of the materials. The spectroscopic/thermal analyses revealed that the hollow Nd/TiO_2 sub-microspheres had a higher surface area and higher temperature requirement for the anatase-to-rutile phase transformation.

Acknowledgements

The authors wish to thank the Research Innovation Program for College Graduates of Qiqihar University (YJSCX2016-ZD05) for financial support. In addition, the authors also would like to express their gratitude to Research Project of the Ministry of Human Resources and Social Security of China (2015) for financial support.

Notes and references

1 P. K. Sanoop, S. Anas, S. Ananthakumar, R. Saravanan and V. Ponnusami, *Arabian J. Chem.*, 2016, **9**, 1618–1626.
2 Y. Li, L. F. Wang, J. Ge, J. Wang, Q. Y. Li, W. Wan, B. P. Zhang, X. G. Liu and W. D. Xue, *RSC Adv.*, 2016, **6**, 106508–106515.
3 R. Lei, H. W. Ni, R. S. Chen, B. W. Zhang, W. T. Zhan and Y. Li, *Chem. Phys. Lett.*, 2017, **673**, 1–6.
4 L. Renuka, K. S. Anantharaju and S. C. Sharma, *J. Alloys Compd.*, 2017, **695**, 382–395.
5 G. Poungchan, B. Ksapabutr and M. Panapoy, *Mater. Des.*, 2016, **89**, 137–145.
6 F. Hoshyargar, H. Khan, K. Kalantar-Zadeh and A. P. O'Mullane, *Chem. Commun.*, 2015, **51**, 14026–14029.
7 M. Babaeia, C. Dehghaniana and P. Taheri, *Surf. Coat. Technol.*, 2016, **307**, 554–564.
8 K. Gurushantha, K. S. Anantharaju, L. Renuka, S. C. Sharma, H. P. Nagaswarupa, S. C. Prashantha, Y. S. Vidya and H. Nagabhushana, *RSC Adv.*, 2017, **7**, 12690–12703.
9 K. Kalantar-Zadeh, J. Z. Ou, T. Daeneke, A. Mitchell, T. Sasaki and M. S. Fuhrer, *Applied Materials Today*, 2016, **5**, 73–89.
10 J. Y. Shi, Y. Kuwahara, T. C. An and H. Yamashita, *Catal. Today*, 2017, **281**, 21–28.
11 X. F. Zhang, Y. N. Wang, B. S. Liu, Y. H. Sang and H. Liu, *Appl. Catal., B*, 2017, **202**, 620–641.
12 Z. Y. Zhang, X. Chang and A. C. Chen, *Sens. Actuators, B*, 2016, **223**, 664–670.
13 Z. G. Bai, Y. Hu, S. Q. Yan, W. J. Shan and C. H. Wei, *RSC Adv.*, 2017, **7**, 1966–1974.
14 J. L. Li, T. Liu, G. Z. Sui and D. S. Zhen, *J. Nanosci. Nanotechnol.*, 2015, **15**, 1408–1415.
15 C. Matteo, T. R. Gordon and C. B. Murray, *Chem. Rev.*, 2014, **114**, 9319–9345.
16 T. J. Zhu, J. Li and Q. S. Wu, *ACS Appl. Mater. Interfaces*, 2011, **3**, 3448–3453.
17 X. Q. Meng, X. Z. Wang, M. Z. Zhong, F. G. Wu and Y. Z. Fang, *J. Solid State Chem.*, 2013, **201**, 75–78.
18 D. G. Xiang, Y. Y. Li and Z. W. Lin, *Appl. Surf. Sci.*, 2013, **270**, 457–461.
19 Y. J. Wang, S. Yang and H. G. Lee, *Appl. Catal., B*, 2017, **204**, 209–215.
20 C. Marien, T. Cottineau and D. Robert, *Appl. Catal., B*, 2016, **194**, 1–6.
21 A. Bjelajac, R. Petrovic, G. Socol, I. N. Mihailescu, V. Grumezescu and V. Pavlovic, *Ceram. Int.*, 2016, **42**, 9011–9017.
22 S. Pal, A. M. Laera and L. Antonio, *Ind. Eng. Chem. Res.*, 2014, **19**, 7931–7938.
23 J. Du, H. J. Chen, H. Yang, R. Sang, Y. T. Qian, Y. X. Li, G. G. Zhu, Y. J. Mao, W. He and D. J. Kang, *Microporous Mesoporous Mater.*, 2013, **182**, 87–94.
24 J. J. Yuan, X. K. Zhang, H. D. Li, K. Wang, S. Y. Gao, Z. Yin, H. J. Yu, X. R. Zhu, Z. Z. Xiong and Y. M. Xie, *Catal. Commun.*, 2015, **60**, 129–133.
25 J. Yang, X. H. Wang, J. Dai and J. T. Li, *Ind. Eng. Chem. Res.*, 2014, **53**, 12575–12586.
26 W. J. Tseng and P. S. Chao, *Ceram. Int.*, 2013, **39**, 3779–3787.
27 R. Wang, X. Cai and F. L. Shen, *Ceram. Int.*, 2013, **39**, 9465–9470.
28 T. Leshuk, S. Linley and G. Baxter, *ACS Appl. Mater. Interfaces*, 2012, **4**, 6062–6070.

29 W. W. Wang, D. Zhu, Z. Shen and X. H. Liu, *Ind. Eng. Chem. Res.*, 2016, **55**, 6373–6383.
30 W. Zhang, J. Z. Ou, S. Y. Tang, V. Sivan, D. D. Yao, K. Latham, K. Khoshmanesh, A. Mitchell, A. P. O'Mullane and K. Kalantar-Zadeh, *Adv. Funct. Mater.*, 2014, **24**, 3799–3807.
31 B. Wang, G. X. Zhang, Z. M. Sun, S. L. Zheng and R. L. Frost, *J. Environ. Chem. Eng.*, 2015, **3**, 1444–1451.
32 Y. Q. Wang, H. M. Cheng, L. Zhang, Y. Z. Hao, J. M. Ma, B. Xu and W. H. Li, *J. Mol. Catal. A: Chem.*, 2000, **151**, 205–216.
33 P. Margan and M. M. Haghighi, *J. Sol–Gel Sci. Technol.*, 2017, **81**, 556–569.
34 P. Zhang, Y. L. Yu, E. J. Wang, J. S. Wang, J. H. Yao and Y. A. Cao, *ACS Appl. Mater. Interfaces*, 2014, **6**, 4622–4628.
35 J. M. Valero, S. Ogón and G. Colón, *ACS Catal.*, 2014, **4**, 3320–3329.
36 J. Du, X. Gu, Q. Wu, J. Liu, H. Z. Guo and J. G. Zou, *Trans. Nonferrous Met. Soc. China*, 2015, **25**, 2601–2607.
37 X. L. Wang, H. Y. Yin and Q. L. Nie, *Mater. Chem. Phys.*, 2017, **185**, 143–151.
38 D. Bu and H. S. Zhuang, *Catal. Commun.*, 2012, **29**, 24–28.
39 W. W. Wang, D. Zhu, Z. Shen, J. Peng, J. Luo and X. H. Liu, *Ind. Eng. Chem. Res.*, 2016, **55**, 6373–6383.
40 N. Seifvand and E. Kowsari, *Ind. Eng. Chem. Res.*, 2016, **55**, 10533–10543.
41 R. Kumar, S. Govindarajan, R. K. Janardhana, T. N. Rao, S. V. Joshi and S. Anandan, *ACS Appl. Mater. Interfaces*, 2016, **8**, 27642–27653.
42 R. Liu, P. Wang, X. F. Wang, H. G. Yu and J. G. Yu, *J. Phys. Chem. C*, 2012, **116**, 17721–17728.
43 X. Y. Wu, S. Yin, Q. Dong, C. S. Guo, T. Kimura, J. I. Matsushita and T. Sato, *ACS Appl. Mater. Interfaces*, 2013, **117**, 8345–8352.
44 X. W. Cheng, X. J. Yua, Z. P. Xing and J. F. Wan, *Energy Procedia*, 2012, **16**, 598–605.
45 S. K. Parayil, H. S. Kibombo, C. M. Wu, R. Peng, J. Baltrusaitis and R. T. Koodali, *Int. J. Hydrogen Energy*, 2012, **37**, 8257–8267.
46 X. J. Huang, X. Yan, H. Y. Wu, Y. Fang, Y. H. Min, W. S. Li, S. Y. Wang and Z. J. Wu, *Trans. Nonferrous Met. Soc. China*, 2016, **26**, 464–471.
47 L. G. Devi and R. Kavitha, *Appl. Surf. Sci.*, 2016, **360**, 601–622.
48 R. P. Cavalcante, R. F. Dantas, B. Bayarri, O. González, J. Giménez, S. Esplugas and A. M. Junior, *Appl. Catal., B*, 2016, **194**, 111–122.